THE JOURNAL OF PHYSICAL CHEMISTRY A

Article

pubs.acs.org/JPCA

Understanding the Structure and Electronic Properties of Molecular Crystals Under Pressure: Application of Dispersion Corrected DFT to Oligoacenes

Bohdan Schatschneider,*[,†] Stephen Monaco,[†] Alexandre Tkatchenko,[‡] and Jian-Jie Liang[§]

[†]The Pennsylvania State University, Fayette-The Eberly Campus, 2201 University Dr, Lemont Furnace, Pennsylvania 15456, United States

[‡]Fritz-Haber-Institut der Max-Planck-Gesellschaft, Faradayweg 4-6, D-14195 Berlin, Germany

[§]Accelrys Inc., 10188 Telesis Court, Suite 100, San Diego, California 92121, United States

Supporting Information

ABSTRACT: Oligoacenes form a fundamental class of polycyclic aromatic hydrocarbons (PAH) which have been extensively explored for use as organic (semi) conductors in the bulk phase and thin films. For this reason it is important to understand their electronic properties in the condensed phase. In this investigation, we use density functional theory with Tkatchenko–Scheffler dispersion correction to explore several crystalline oligoacenes (naphthalene, anthracene, tetracene, and pentacene) under pressures up to 25 GPa in an effort to uncover unique electronic/optical properties. Excellent agreement with experiment is achieved for the pressure dependence of the crystal structure unit cell parameters, densities, and intermolecular close contacts. The pressure dependence of the band gaps is investigated as well as the pressure induced phase transition of tetracene using both generalized gradient approximated and hybrid functionals. It is concluded that none of the oligoacenes investigated become conducting under elevated pressures, assuming that the molecular identity of the system is maintained.

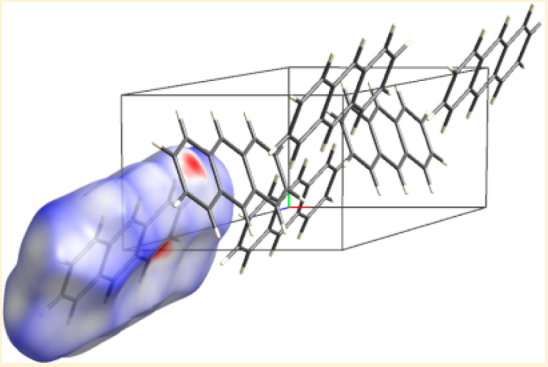

1. INTRODUCTION

Oligoacenes are a class of molecular crystals that have been extensively investigated, both experimentally and theoretically, due to their promising electro-optical properties. The large amount of experimental properties data (X-ray, vibrational/optical spectroscopy, material application, etc.) available in the literature makes these materials excellent benchmarks for computational methods.

In the past, pressure has been used to reduce the resistivity of these semiconductors, suggesting that oligoacences could be the first single component organic molecular crystals (OMC) to show "metallic" behavior.[1] The idea that oligoacenes (particularly pentacene) under pressure are conductors is perpetuated in recent articles[2] and reviews.[3,4] However, a high pressure optical study of pentacene up to ~32 GPa[5] showed no metallization due to condensation reactions, though a steady narrowing of the HOMO–LUMO band gap was observed until the molecular identity of the acene components was compromised.

The pressure dependent narrowing of the band gap in the oligoacenes and other monomolecular OMCs[6] presents the possibility that a semiconducting single component organic system could exhibit conductance under pressure, but predicting which structures to investigate experimentally is a daunting challenge as the pool of potential materials is enormous. Therefore, it would be valuable to have a computational method that can be used in a high-throughput scenario to accurately predict the pressure induced structural changes of OMCs as well as the corresponding electronic and optical properties. In an effort to establish a consistent methodology for the optimization of OMCs under varying thermodynamic conditions, we employ Tkatchenko–Scheffler dispersion corrected density functional theory (PBE+vdW) to observe the pressure induced changes in the structural and electronic properties of naphthalene (2A), anthracene (3A), tetracene (4A), and pentacene (5A).

Many attempts at modeling the acene family have been made, with an aim to understand the lattice dynamics, optical properties, etc. [refs 7–18 and many more]. In regard to the present study, the high pressure exploration of 3A–5A[19,20] is one of the most relevant: In this investigation quasi harmonic lattice dynamics (QHLD) using classical potentials were combined with Raman spectroscopy and X-ray experiments to understand the pressure response of unit cell dimensions and

Received: July 3, 2013
Revised: July 24, 2013
Published: July 31, 2013

Table 1. Unit Cell Parameters from Low Temperature X-ray and PBE+vdW Calculation[a]

	low temperature X-ray				PBE+vdW			
	a (Å)	b (Å)	c (Å)	ρ (g/mL)	a (Å)	b (Å)	c (Å)	ρ (g/mL)
naphthalene (NAPHTA06 [92 K])	8.108	5.94	8.647	1.239	8.117	5.897	8.647	1.244
anthracene (ANTCEN09 [92 K])	8.414	5.99	11.095	1.297	8.399	5.906	11.12	1.313
tetracene (TETCEN01 [175 K])	6.056	7.838	13.01	1.323	6.050	7.706	13.030	1.343
pentacene H (PENCEN04 [90 K])	6.239	7.636	14.333	1.397	6.129	7.676	1.531	1.392
C (PENCEN [298 K])	(7.900)	(6.060)	(16.010)	(1.335)	(7.658)	(6.040)	(15.847)	(1.3887)

[a]Cambridge Structural Database (CSD) Refcodes are in parentheses. Temperature of the x-ray structure is in brackets. Pentacene has two polymorphs, H and C; Parentheses in the pentacene row corresponds to values for polymorph C which is an entirely different structure than H, not merely the same structure after thermal expansion.

the vibrational modes. Good agreement was achieved between the modeling and experiment. However, the calculations assumed rigidity of the molecules under increased pressure, which may not be true as other "rigid" PAHs[29] have been shown to be flexible under high pressures. Also, transferability of interaction parameters developed for structures under ambient condition may cause problems when used under pressure. It is also of interest to note that the X-ray data in the original study was not of sufficient resolution for a detailed structure study (refinement) to validate the transferability.

Previously, we investigated the role of including 2-body (PBE+vdW) vs. many-body (PBE+MBD) dispersion correction in the calculation of sublimation energies and dielectric constants for 2A−5A.[21] It was ultimately concluded in that study,[21] as well as others,[22,23] that the 2-body Tkatchenko−Scheffler (PBE+vdW) dispersion correction is an excellent method for modeling crystal structures but that a many body method, such as PBE+MBD, is necessary for deciphering between the small energetic differences associated with calculating the lattice binding energies. Consequently, if one wishes to explore only structure, PBE+vdW is sufficient, but if calculations of energetic/electronic properties resulting from intermolecular interactions are required, the inclusion of many body effects is necessary.

Though several methodologies have been applied to understand 2A−5A, none have been universally applicable for the investigation of thermochemical, kinetic, and optical properties in the condensed phase. Also, while several different dispersion corrected DFT schemes have shown promise in calculating large sets of OMC structures and properties under ambient pressure conditions,[22,24,25] the methods have yet to show promise in application to the dynamic nature of molecular crystals under high pressure. Here, we take steps toward providing a reliable DFT method for modeling OMCs under a variety of thermodynamic conditions.

2. COMPUTATIONAL DETAILS

Density functional theory[26] implemented in the program CASTEP[27] was used in this investigation. Starting structures of each acene were obtained from the lowest temperature data sets available in the Cambridge Structural Database (CSD). The low temperature polymorphs were chosen for tetracene and pentacene. The pressure was increased in 0.5 GPa steps. The structure at each pressure was geometry optimized using the BFGS minimizer within CASTEP which uses a starting Hessian that is recursively updated during optimization.[28] Implementation of BFGS within CASTEP involves a Hessian in the mixed space of internal and cell degrees of freedom. This results in the optimization of both lattice parameters and atomic coordinates.

Norm-conserving potentials were utilized for C, where valence electrons included $2s^2$ and $2p^2$ states. The planewave basis set cutoff was 750 eV. The use of a relatively high plane wave basis set cutoff is to ensure that the total energy and unit cell volume converge, as demonstrated in a similar study of crystalline indole[29] and 2A−5A.[21] The k-point grid was kept to maintain a spacing of ca. 0.07 $Å^{-1}$. The GGA functional of Perdew, Burke, and Ernzerhof (PBE)[30] was employed. The convergence criteria for total energy, max force, max stress, max displacement, and SCF iterations were 5×10^{-6} eV/atom, 0.01 eV/Å, 0.02 GPa, 5×10^{-4} Å and 5×10^{-7} eV/atom, respectively.

An essentially nonempirical method, introduced by Tkatchenko and Scheffler (TS),[31] was used to add the pervasive van der Waals (vdW) interactions common in molecular crystals which are missing in the PBE functional. In the TS method, the polarizability, C_6 coefficients, and vdW radii are determined from the Hirshfeld partitioning of the self-consistent electron density of the crystal.[31] Unlike other empirically derived dispersion corrections, the C_6 coefficients and polarizabilities of the TS scheme will change with pressure as the electron density, and consequently Hirshfeld partitioning, changes.

There has been a surge of different methods within the past decade which aim at accounting for vdW interactions in quantum mechanical treatment of materials systems. Each approach in this large collection has its own advantages and shortcomings. We defer our readers to a recent comprehensive review on the various methods.[32] The choice of the present scheme of vdW correction is to continue our systematic effort[21,28,33] in validating/further developing the methodology that (a) is generally applicable and scalable to extended solid state systems and (b) yields remarkable accuracy for intermolecular interactions, of 8% error for energies and 0.1 Å for equilibrium distances.

Band gaps were calculated with PBE, HSE03, and PBE0 functionals on the PBE+vdW geometry optimized structures while maintaining all other convergence criteria as above. The hybrid PBE0 functional was used as a remedy for the underestimation of the band gap by PBE.[13,14,34]

Hirshfeld surfaces and fingerprint plots were produced in the program Crystal Explorer.[35] Hirshfeld surfaces represent the surface space occupied by a molecule's electron density as derived from the 0.5 isosurface of the weight function, $w_A(\mathbf{r})$, where the vdW radii are derived from Bondi.[36,37] Fingerprint plots are a 2D representation of the deconvoluted Hirshfeld surface; that is, for each point on the Hirshfeld surface, the contact of the internal (d_i) and external nuclei (d_e) with the surface is determined. Each unique d_e and d_i pair is represented by a point on the 2D fingerprint plot. The color of each point on the fingerprint plot corresponds to the relative area

associated with a d_e and d_i pair. This provides for the quantitative measurement of intermolecular close contacts. Detailed explanations of the Hirshfeld surface and fingerprint plots can be found in refs 35-37.

The present structural study corresponds to static energy minimizations (0 K temperature) using TS pairwise dispersion correction. While recent studies[21,38,39] suggest that a many body approach is necessary for the realistic calculation of the intermolecular cohesive energies, the TS method has been shown to reliably model the structures and energetics of other OMCs under ambient and high pressure conditions.[22,23,29,33] As a result, PBE+vdW is implemented for all structural minimizations.

3. RESULTS AND DISCUSSION

3.1. Ambient Pressure. *3.1.1. Structure.* The ability of the PBE+vdW method to accurately model the crystalline structures of the oligoacene series is demonstrated in Tables 1 and 2. The lowest temperature X-ray data was specifically chosen as the initial structure in the present study to minimize thermal expansion effects between the calculated and experimental structures (as DFT optimizes at 0 K).

Table 2. Intermolecular Close Contact Interactions As Calculated from Hirshfeld Surfaces[a]

	low temperature X-ray			PBE+vdW		
	C···C%	C···H%	H···H%	C···C%	C···H%	H···H%
naphthalene (NAPHTA06 [92 K])	0.4	46.9	52.7	0.4	46.9	52.7
anthracene (ANTCEN09 [92 K])	1.1	51.0	47.8	1.2	52.0	46.9
tetracene (TETCEN01 [175 K])	0.5	56.2	43.3	0.7	58.1	41.2
pentacene (PENCEN04 [90 K])	0.4	61.4	38.2	0.5	59.7	39.8

[a]CSD Refcodes are in parentheses. Temperature of the X-ray structure is in brackets. Error for the % is ±0.2%.[41].

It is known that dispersion interactions do not play a large role in the calculation of the (intra-) molecular geometry within the crystal lattice when the unit cell parameters are held constant,[40] but no dynamic response of the lattice to temperature or pressure can be obtained using this method. In the present work, using the PBE+vdW method, good agreement between the calculated and experimental molecular structures is still retained (see Figure A in the Supporting Information): All C−C distances are within 2% of experiment, and H−C distances are within ∼10% (due to the well-known fact that X-ray structure determination gives shortened bond length for polar bonds, where the centers of the electron densities become closer than the positions of the corresponding nuclei). The correlation of the calculated and experimental crystal structures is presented in Table 1. It is worth pointing out that ≤2% variations in unit cell parameters compared to experimental is achieved; this is otherwise not possible without vdW correction.

To exemplify the increase in correlation when using the low temperature structures, the high and low temperature polymorphs of 5A (C and H)[8] are compared in Table 1. The high temperature data of polymorph C of 5A is within ∼4% of experiment while that of the low temperature data of polymorph H is within 1%. It is important nowadays to have such tight tolerances between experimental and calculated values as so much emphasis is put on the ability to calculate sublimation enthalpies of these systems; where small variations in the structure can lead to large variations in the intermolecular cohesive energies.

While comparison of the unit cell parameters and density for the calculated and experimental structures aides in understanding whether a calculated structure has realistic distances between the molecules, it is also important to assess if the calculated intermolecular interactions are similar to what exists within the experimental structure. Hirshfeld surfaces can answer this question by providing a quantitative measure of intermolecular close contacts by sampling the electron density surrounding each molecule, and correlating the intermolecular close contacts occurring at the surface to specific atom types.[29,33,35−37,41] Hirshfeld surfaces enable the construction of a "2D fingerprint plot" which demonstrates specific atom−atom intermolecular interactions, providing a quantitative value to the fraction of a given contact type at the surface with respect to all others. The intermolecular close contact fractions for the ambient pressure structures are demonstrated in Table 2, showing excellent agreement between the intermolecular orientations of the calculated and experimental structures.

3.2. High Pressure. *3.2.1. 2A and 3A.* Oligoacenes have been extensively studied under a variety of thermodynamic conditions where interesting optical/conductive properties are expected to emerge. High pressure conditions are of specific interest as one may tune the optical properties of these materials, directly altering the conductivity/resistivity due to increased overlap of adjacent molecules within the unit cell.[42] The ability of PBE+vdW to model the pressure induced structural changes of oligoacene crystals as observed via X-ray diffraction is demonstrated in Figures 1−3. The structural response of 2A and 3A up to 25 GPa is shown in Figure 1, and excellent agreement with experiment is obtained for the unit cell parameters. Further structural correlation beyond the unit cell parameters is shown in Figure 1 through the interplanar[43]/herringbone angle[19] (θ) of 3A.

The response of the intermolecular close contacts as a function of pressure for 2A and 3A is shown in Figure 2, demonstrating that as pressure increases, the fraction of H···H interactions decrease while the C···H and C···C interactions increase (similar to the changes observed in pressurized indole[29]). This is the direct result of the increase in θ,[19,20] which yields more efficiently packed structures by increasing the fraction of C···C (π···π stacking) and C···H contacts and decreasing the amount of H···H close contacts.

3.2.2. 4A. "Polymorph I"[7] (TETCEN01) of 4A was chosen for investigation under high pressure as (a) it undergoes a phase transition above 6 GPa[7] to a phase possessing similar Raman lattice phonon lines to "polymorph II"[7,45] and (b) it was used in high pressure X-ray experiments[20] which are useful benchmarks. It should be noted that though numerous pressure induced phase transitions have been reported for 4A (besides the 6 GPa transition from phase I to II), the newest pressure dependent Raman data[7] and our results do not confirm these transitions.

The unit cell parameters, θ, and the intermolecular close contacts as a function of pressure for 4A are shown in Figures 2 and 3 up to 24 GPa. Comparison with experiment[20] shows good agreement for the unit cell parameters. PBE+vdW reveals

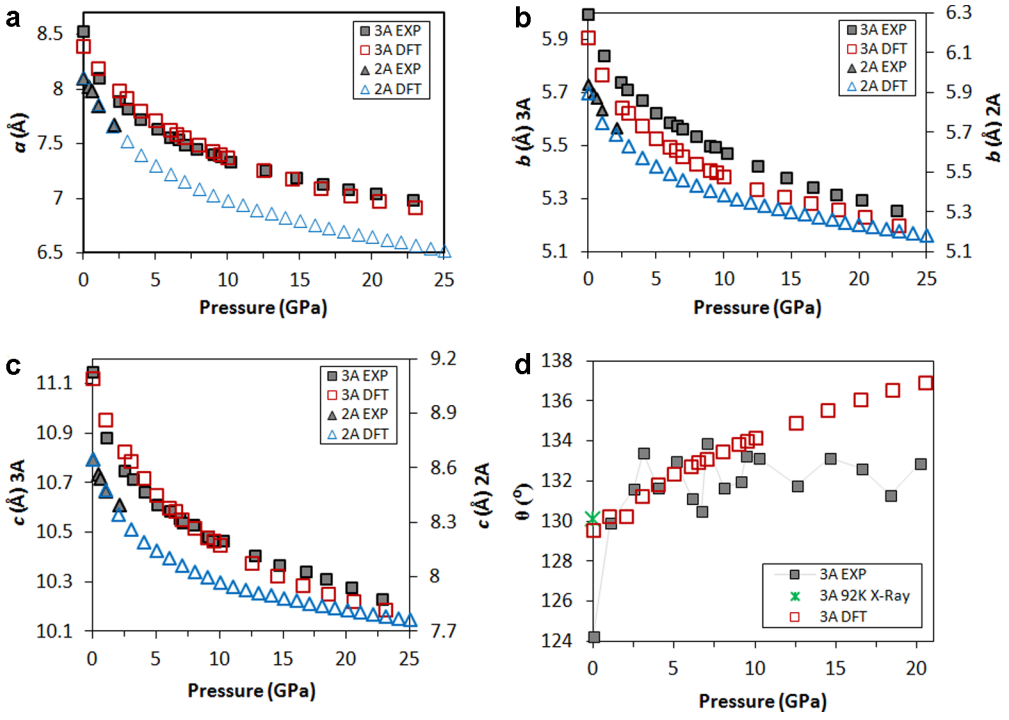

Figure 1. Unit cell parameters and interplanar angles of 2A[44] and 3A[19] as a function of pressure from powder X-ray and PBE+vdW. In (d), "EXP" θ values are from,[20] 92 K θ value at 0 GPa is from ANTCEN09. b and c of 2A are on the secondary axis for clarity.

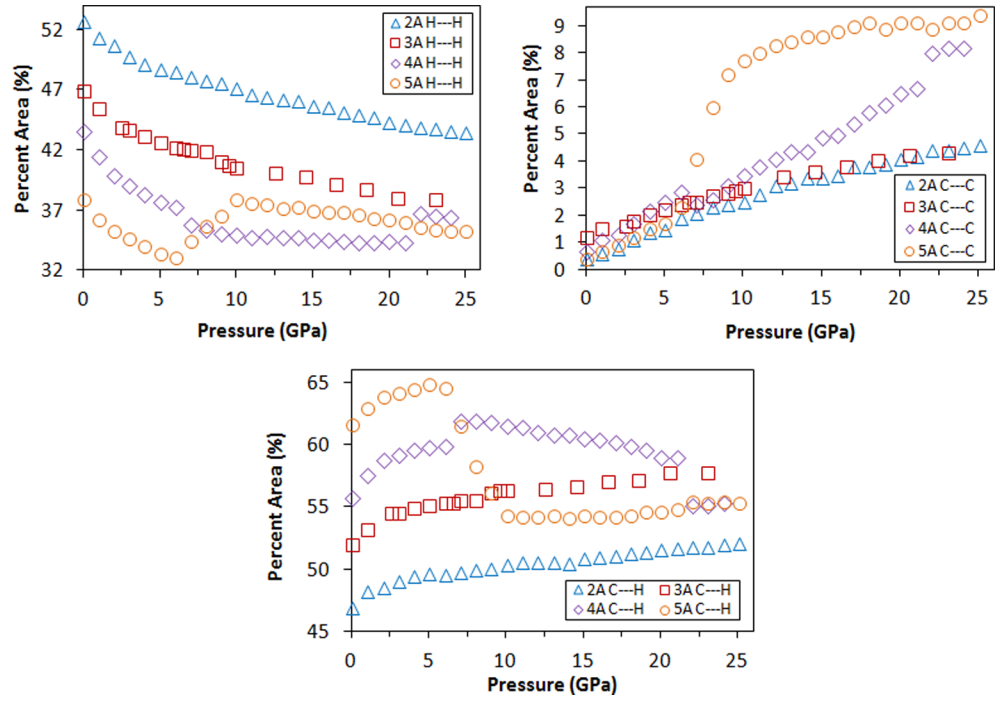

Figure 2. Relative contributions to the Hirshfeld surface area for the intermolecular close contacts as a function of pressure for 2A−5A. Error for the % is ±0.2%.[41]

discontinuities in the unit cell parameters, intermolecular close contacts, and θ between 6 and 7 GPa (this is indicative of a phase transition as we will explain). Similar discontinuities are also observable in the experimental parameters of Figure 3 (though not noted in the original manuscript[20]). While previous classical QHLD calculations[20] reasonably modeled the unit cell parameters of 4A as a function of pressure, no notable structural rearrangements indicative of a phase transition were reported from these simulations (possibly the result of the rigid molecule assumption).

There is no change in the symmetry or motif[41] of the crystal associated with the calculated discontinuities (also observed in comparison with the experimental structures of the two phases[7]). The structural rearrangement increases the packing efficiency by increasing θ. This increases the C···C and C···H contacts while limiting the H···H contacts (detailed in Figure b

dx.doi.org/10.1021/jp406573n | J. Phys. Chem. A 2013, 117, 8323−8331

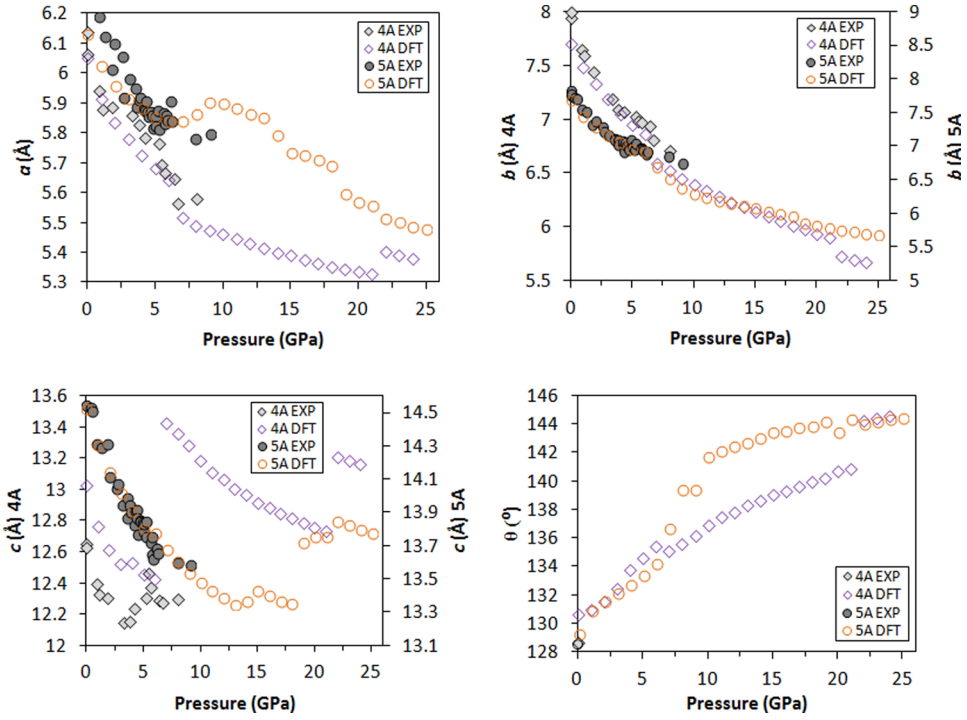

Figure 3. Unit cell parameters and θ of 4A and 5A as a function of pressure from X-ray[20] and PBE+vdW. The low temperature θ values are from TETCEN01 and PENCEN04 (polymorph H).

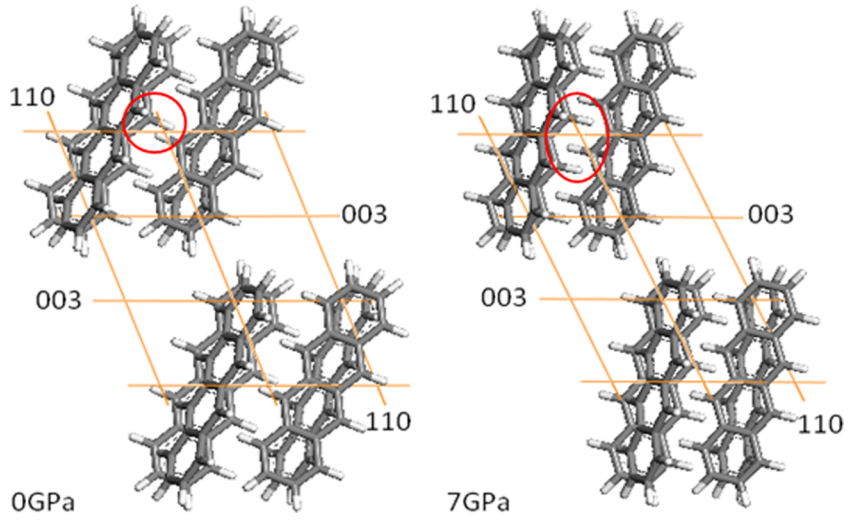

Figure 4. Molecular arrangement of 4A before and after the phase transition at 0 and 7 GPa. Red circles emphasize the shift between interlocking hydrogens.

of the Supporting Information). Between 0 and 6 GPa, the structure compresses anisotropically (despite the isostatic pressure conditions). The compression ratio with increasing pressure is 6.8%, 11.0%, and 4.6% along *a*-, *b*-, and *c*-cell dimensions respectively. The phase transition can then be characterized by a sudden increase in the *c*-dimension and a 2.2% density increase from 1.685 to 1.722 g/mL, while atomistically, the phase transition corresponds to a change/shift in stacking patterns in the molecular crystal. As illustrated in Figure 4, the stacking shift is along the molecular axis, where the interlocking hydrogens shift along the long molecular axis by about one-quarter of the repeating distance.

The phase transition can also be characterized by a relatively subtle but important structure change in the position of the 110 reflection in the powder X-ray diffraction (PXRD) pattern (see Figure 5). At ambient pressure, the 2θ position of 110 is of lesser magnitude than those of the near-degenerate $1\bar{1}0/112$ reflections. The relative position remains unchanged up to 6 GPa, but at the phase transition, the position of the 110 reflection moves significantly higher (by 1.82° 2θ). This corresponds to a sudden decrease in *d*-spacing from 4.23 Å at 6 GPa to 3.85 Å at 7 GPa. The phase transition can therefore be characterized by a simultaneous increase in the *c*-dimension and a decrease in the 110 *d*-spacing (also refer to Figure 4). These structural changes appear frozen-in after the structure is quenched to ambient pressure (see Figure 5).

Another important point to emphasize with regard to the phase transition is the change in the intramolecular structure.

dx.doi.org/10.1021/jp406573n | J. Phys. Chem. A 2013, 117, 8323−8331

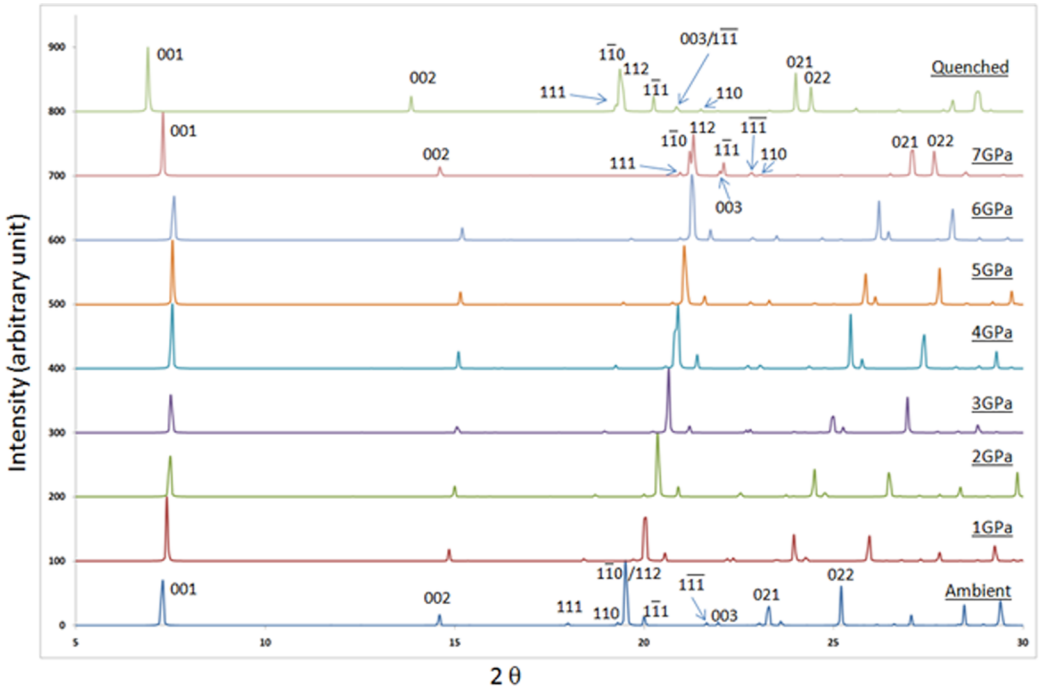

Figure 5. Simulated powder X-ray diffraction patterns of 4A under increasing isostatic pressure.

Figure 6 shows the C−H and C−C bond distance distribution through radial distribution function (RDF) analysis, and its evolution as a function of applied pressure. It is evident that immediately after the phase transition at 7 GPa, the C−C bond distance distribution changes significantly; that is, there is a more pronounced split for the two groups of C−C bond distances, one centered at 1.37 and the other at 1.43 Å, respectively. Moreover, the shorter C−C bond distances (centered at 1.37 Å) become prominent, which is reversed before the transition.

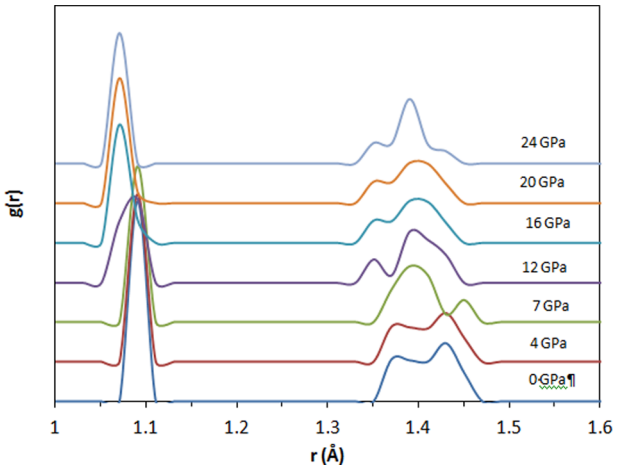

Figure 6. Radial distribution function of 4A as a function of pressure.

It is interesting to note that the intermolecular close contacts of 4A undergo different trends than 2A and 3A in Figure 2. While the C···C contacts have an overall increase over all pressures (similar to 2A and 3A), the C···H contacts do not (initially increasing until 8 GPa followed by steady decrease). The H···H contacts also vary from the 2A and 3A trends in that they stop decreasing after 9 GPa in 4A, leveling off at a 34.5% limit. These variations likely occur as 4A is an inherently different structure than 2A and 3A (being triclinic instead of monoclinic).[20,46]

It is noted that a second discontinuity is observed between 21 and 22 GPa in all parameters of 4A in Figures 2 and 3. In-depth characterization of this discontinuity was not performed as it occurs at pressures where the identity of the 4A molecules is expected to be compromised due to condensation reactions;[5,47] this is beyond the scope of the present effort.

3.2.3. 5A. The present work focuses exclusively on the more stable polymorph H of 5A. The response of the unit cell parameters and θ as a function of pressure for polymorph H of 5A are shown in Figure 3. Good correlation with the X-ray data is observed for all parameters and θ. The symmetry and motif were maintained across all pressures as in experiment.[5]

The reaction of 5A to pressure, particularly the intermolecular close contacts, is quite different than those of 2A and 3A, as seen in Figure 2. This is most likely due to symmetry differences, where 5A is triclinic and 2A/3A are monoclinic. There are notable discontinuities in the a unit cell parameter and θ above 6 GPa resulting in discontinuous changes in the intermolecular close contacts. The increase in θ allows for efficient molecular packing at a faster rate than the other acenes. An explanation for this could be supplied by previously DFT-D calculations[46] which showed that there is an increased likelihood of π-stacking as the number of rings increases. This π-stacking trend can be further corroborated as there is an increased pressure dependence of the C···C contacts when proceeding from 2A−5A in Figure 2.

The fraction of C···H and H···H contacts also have inflections in Figure 2 starting at 6 GPa, with the C···H contacts decreasing and the H···H contacts increasing. The decrease in the C···H contacts and increase in H···H contacts is opposite in trend to the other acenes, owning to the unique pressure dependent properties that 5A possesses.

3.3. Oligoacene Band Gap Pressure Dependence. As mentioned, OMCs have shown promise for use in electronics,

dx.doi.org/10.1021/jp406573n | J. Phys. Chem. A 2013, 117, 8323−8331

but in order to predict whether an OMC has potential use as a (semi-) conductor, experiments must be carried out to ensure the viability of the material. Rational selection of new materials to investigate is critical for efficient materials development, and accurate prediction of the band structure would be valuable before experiments are conducted. The need for cheaper, flexible electronic materials creates a pressing need for band gap engineering; that is, mapping out factors and their control over band gap variation for a given material is of prime interest.

It is known that calculation of the band structure for conducting OMCs is somewhat routine.[48] On the other hand, the calculation of the band gap for semiconducting OMCs is problematic using DFT due to insufficient description of the exchange/correlation interactions. Despite the fact that DFT (particularly PBE) underestimates the band gaps of oligoacences (and other OMCs), it can typically reproduce electronic trends within families of molecules (e.g., oligoacenes).[13,14]

Given PBEs success in calculating electronic trends in families of molecules, there is still a need to verify/calibrate the DFT band gap variation with more accurate predictions. Various approaches aimed at improving the description of exchange/correlation interactions have been proposed,[34] among which, hybrid PBE0[49] or HSE03[50,51] functionals are of particular importance. These are density functional approximations that combine a PBE generalized gradient functional with a predefined amount of (screened) exact exchange. The absence of adjustable parameters fitted to specific properties makes PBE0 and HSE03 particularly attractive in calculating a large variety of properties for significantly different materials.

The results of calculating the HOMO−LUMO band gap for 2A−5A using PBE and the hybrid PBE0 and HSE03 functionals for the PBE+vdW optimized structures are shown in Table 3.

Table 3. Oligoacene Band Gaps As Calculated Using PBE +vdW, HSE03, and PBE0 (using PBE+vdW Structures) vs Experiment[13,14]

	band gap (E_g) [eV]			
	PBE	HSE03	PBE0	exp
2A	3.007	3.857	4.595	5.0−5.4
3A	1.926	2.615	3.330	3.9−4.2
4A	1.365	1.942	2.659	2.9−3.4
5A	0.858	1.431	2.031	2.2−2.4

While PBE underestimates the band gaps in oligoacenes (between ∼40 and 65% error),[13,14] it does correctly establish the trend of shrinking band gaps upon ring addition. To improve the band gap results, the electronic structure was computed with HSE03 and PBE0 functionals at PBE+vdW geometries. HSE03 provides band gaps with better accuracy than that of PBE (within ∼30%), but PBE0 yields the best agreement with experiment (within ∼8%), providing a pragmatic approach to calculate the band gaps of aromatic molecular crystals.

Since it is known that pressure can be used to alter the optical and electronic properties of semiconducting OMCs, the pressure dependence the of band gaps for 2A-5A was investigated up to 30 GPa as shown in Figure 7. 2A and 3A are not known to be conductive under high pressure, and neither undergoes a phase transition up to 30 GPa. This is reflected in the near linear response of the band gap to pressure.

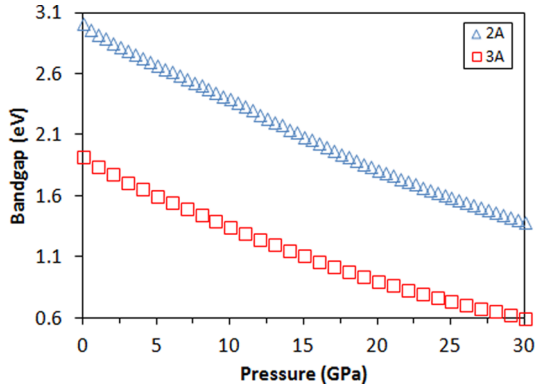

Figure 7. HOMO−LUMO band gap as function of pressure for 2A and 3A as calculated with PBE.

As mentioned above, 4A undergoes a phase transition under high pressures. This phase transition can be further observed in the discontinuity in the band gap pressure dependence between 6 and 7 GPa in Figure 8a. 4A is not known to be a conductor under high pressure[1,52] and is likely to undergo condensation reactions at high pressures (>10 GPa).[47] Nonetheless, PBE predicts that the band gap will go to zero by 17 GPa (see Figure 8a). As explained earlier, PBE severely underestimates the band gaps in organic materials, therefore we investigated the band gap pressure dependence with PBE0 as shown in Figure 8a. It can be seen that, when the band gap pressure dependence is calculated with PBE0, the narrowing of the band gap stops at 0.4 eV and levels off in a similar manner to previous resistivity measurements.[1]

Particular attention was paid to 5A as it is a semiconductor under ambient conditions but was shown to become "metallic" below 200 K and 27.0 GPa.[1] In the face of the metallization findings,[1] more recent investigations at room temperature[5] show that an amorphous product is produced between 8 and 11 GPa due to condensation reactions and that the loss of molecular identity halts the band gap closure. Figure 8b demonstrates the band gap of 5A shrinking as a function of pressure as calculated *via* PBE, HSE03, and PBE0. All calculations result in a similar trend; that is, the band gap continuously decreases as a function of applied pressure up to 18 GPA before subsequent expansion.

The decrease of the band gap in the more quantitative PBE0 and HSE03 calculations are on the order of −0.09 and −0.07 eV/GPa, respectively. This correlates well with the −0.08 eV/GPa decrease in the HOMO−LUMO transition energies observed experimentally via optical absorption measurements.[5] Linear extrapolation of the band gap vs pressure relationship for PBE0 in Figure 8b would have the band gap collapse to zero at ∼24 GPa, in good agreement with the 27 GPa loss of resistivity (metallization) observed for 5A below 200 K.[1] However, the band gap never goes to zero for the hybrid functional calculations. This is in qualitative agreement with the band gap narrowing and expansion observed in figure 4b of ref 5. The expansion of the band gap in the experiment is believed to be due to the loss of molecular identity within the structure where an amorphous product is produced between 8 and 11 GPa due to condensation reactions.[5] The present study reveals that the band gap expansion may have a more fundamental origin within the pentacene structure under high isostatic pressure, which may be confirmed experimentally if pressure-induced condensation/amorphization can be prevented. On the

dx.doi.org/10.1021/jp406573n | J. Phys. Chem. A 2013, 117, 8323−8331

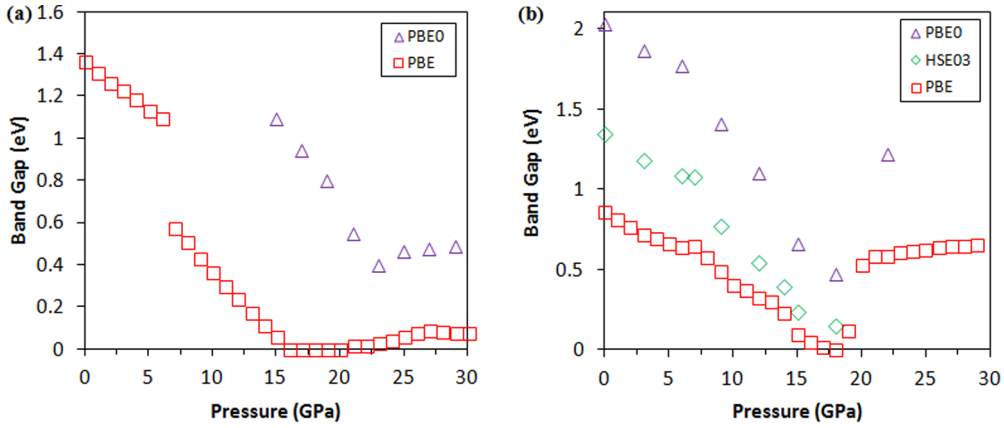

Figure 8. 4A and 5A HOMO−LUMO band gap as function of pressure. (a) 4A band gap pressure dependence as calculated with PBE and PBE0. (b) 5A band gap pressure dependence as calculated with PBE, HSE03, and PBE0.

other hand, further computational studies may model the aforementioned condensation reactions and the associated structural/electronic properties under elevated pressure.

4. CONCLUSION

Tkatchenko−Scheffler dispersion corrected DFT (PBE+vdW method) was used in this investigation to explore several oligoacenes under pressures up to 25 GPa. Excellent agreement between calculated and experiment crystal structures was achieved for ambient and high pressure regimes. The ability of PBE+vdW to dynamically adapt to changes in the chemical environment was demonstrated by the reproduction of the pressure induced phase transitions of tetracene. It was found that good agreement between the calculated and experimental band gaps was achieved when using the PBE0 hybrid functional. It was shown that the metallization of pentacene under high pressures is not expected to occur, in agreement with recent experiment. The good correlation achieved in this investigation demonstrates the versatility of PBE+vdW in the calculation of organic molecular crystal properties, and future high throughput investigations of OMCs using PBE+vdW may uncover several useful low band gap materials.

■ ASSOCIATED CONTENT

Supporting Information

Comparisons of molecular geometries from experiment and calculation as well as detailed Hirshfeld surface analysis information on the phase transition of 4A. This material is available free of charge via the Internet at http://pubs.acs.org.

■ AUTHOR INFORMATION

Corresponding Author

*E-mail: bxs54@psu.edu. Phone: (724) 430-4257.

Notes

The authors declare no competing financial interest.

■ ACKNOWLEDGMENTS

B.S. would like to thank the Eberly Science Foundation for their ongoing support of this work. J.-j.L. would like to thank Accelrys for the company's continued commitment to sciences.

■ REFERENCES

(1) Aust, R. B.; Bentley, W. H.; Drickamer, H. G. Behavior of Fused Ring Aromatic Hydrocarbons at Very High Pressure. *J. Chem. Phys.* **1964**, *41*, 1856−1864.
(2) Tse, J. S.; Leitch, A. A.; Yu, X.; Bao, X.; Zhang, S.; Liu, Q.; Jin, C.; Secco, R. A.; Desgreniers, S.; Ohishi, Y.; Oakley, R. T. Metallization of a Hypervalent Radical Dimer: Molecular and Band Perspectives. *J. Am. Chem. Soc.* **2010**, *132*, 4876.
(3) Saito, G.; Yoshida, Y. Frontiers of organic conductors and superconductors. *Top. Curr. Chem.* **2012**, *312*, 67−126.
(4) Saito, G.; Yoshida, Y. Development and Present Status of Organic Superconductors *Superconductors: Materials, Properties and Applications*; InTech, 2012; pp 105−136; 10.5772/50424.
(5) Farina, L.; Syassen, K.; Brillante, A.; Della Valle, R. G.; Venuti, E.; Karl, N. Pentacene at High Pressure. *High Press. Res.* **2003**, *3*, 349.
(6) Brillante, A.; Della Valle, R. G.; Farina, L.; Venuti, E.; Cavazzoni, C.; Emerson, A. P.; Syassen, K. High-pressure dissociation of crystalline para-diiodobenzene: optical experiments and Car-Parrinello calculations. *J. Am. Chem. Soc.* **2005**, *127*, 3038.
(7) Venuti, E.; Della Valle, R. G.; Farina, L.; Brillante, A.; Masino, M.; Girlando, A. Phonons and structures of tetracene polymorphs at low temperature and high pressure. *Phys. Rev. B* **2004**, *70*, 104106.
(8) Brillante, A.; Della Valle, R. G.; Farina, L.; Girlando, A.; Masino, M.; Venuti, E. Raman phonon spectra of pentacene polymorphs. *Chem. Phys. Lett.* **2002**, *357*, 32.
(9) Bordat, P.; Brown, R. Structure and molecular dynamics of crystalline and liquid anthracene and naphthalene: Possible transient rotator phase of naphthalene. *J. Chem. Phys.* **2009**, *130*, 124501.
(10) Yamagata, H.; Norton, J.; Hontz, E.; Olivier, Y.; Beljonne, D.; Brédas, J. L.; Silbey, R. J.; Spano, F. C. The nature of singlet excitons in oligoacene molecular crystals. *J. Chem. Phys.* **2011**, *134*, 204703.
(11) Saeki, M.; Akagi, H.; Fujii, M. Theoretical Study on the Structure and the Frequency of Isomers of the Naphthalene Dimer. *J. Chem. Theory. Comput.* **2006**, *2*, 1176.
(12) Murugan, N. A.; Jha, P. C. Pressure dependence of crystal structure and molecular packing in anthracene. *Mol. Phys.* **2009**, *107*, 1689.
(13) Otsuka, Y.; Tsukada, M. Theoretical Study of Crystal Structures and Energy Bands of Polyacene and Pentacene Derivatives. *J. Phys. Soc. Jpn.* **2009**, *78*, 024713.
(14) Hummer, K.; Ambrosch-Draxl, C. Electronic properties of oligoacenes from first principles. *Phys. Rev. B* **2005**, *72*, 205205.
(15) Della Valle, R. G.; Venuti, E.; Brillante, A. Pressure and temperature effects in lattice dynamics: the case of naphthalene. *Chem. Phys.* **1995**, *198*, 79.
(16) Van-Oanh, N.-T.; Parneix, P.; Bréchignac, P. Vibrational dynamics of the neutral naphthalene molecule from a Tight-Binding approach. *J. Phys. Chem. A* **2002**, *106*, 10144.

(17) Cappellini, G.; Malloci, G.; Mulas, G. Electronic excitations of oligoacenes: A time dependent density functional theory study. *Superlattices Microstruct.* **2009**, *46*, 14.
(18) Malloci, G.; Mulas, G.; Cappellini, G.; Joblin, C. Time-dependent density functional study of the electronic spectra of oligoacenes in the charge states −1, 0, +1, and +2. *Chem. Phys.* **2007**, *340*, 43.
(19) Oehzelt, M.; Heimel, G.; Resel, R.; Puschnig, P.; Hummer, K.; Ambrosch-Draxl, C.; Takemura, K.; Nakayama, A. High pressure x-ray study on anthracene. *J. Chem. Phys.* **2003**, *119*, 1078.
(20) (a) Oehzelt, M.; Aichholzer, A.; Resel, R.; Heimel, G.; Venuti, E.; Della Valle, R. G. Crystal structure of oligoacenes under high pressure. *Phys. Rev. B* **2006**, *74*, 104103. (b) See EPAPS Document No. E-PRBMDO-74-028634 for a complete set of lattice constants as a function of pressure as obtained from the experiment as well as from the theoretical calculations. In addition, a table with all calculated angles is supplied. This document can be reached via a direct link in the online article's HTML reference section or via the EPAPS homepage http:// www.aip.org/pubservs/epaps.html.
(21) Schatschneider, B.; Liang, J.-J.; Reilly, A.; Marom, N.; Zhang, G.-X.; Tkatchenko, A. Electrodynamic response and stability of molecular crystals. *Phys. Rev. B* **2013**, *87*, 060104.
(22) Otero-de-la-Roza, A.; Johnson, E. R. A benchmark for non-covalent interactions in solids. *J. Chem. Phys.* **2012**, *137*, 054103.
(23) Voora, V. K.; Al-Saidi, W. A.; Jordan, K. D. An Assessment of the vdw-TS Method for Extended Systems. *J. Chem. Theory Comp.* **2012**, *8*, 1503.
(24) Maschio, L.; Civalleri, B.; Ugliengo, P.; Gavezzotti, A. Intermolecular Interaction Energies in Molecular Crystals: Comparison and Agreement of Localized Møller Plesset 2, Dispersion-Corrected Density Functional, and Classical Empirical Two-Body Calculations. *J. Phys. Chem. A* **2011**, *115*, 11179.
(25) Civalleri, B.; Zicovich-Wilson, C. M.; Valenzano, L.; Ugliengo, P. B3LYP augmented with an empirical dispersion term (B3LYP-D*) as applied to molecular crystals. *CrystEngComm* **2008**, *10*, 405.
(26) Hohenberg, P.; Kohn, W. Inhomogeneous Electron Gas. *Phys. Rev. B* **1964**, *136*, 864.
(27) Clark, S. J.; Segall, M. D.; Pickard, C. J.; Hasnip, P. J.; Probert, M. J.; Refson, K.; Payne, M. C. First principles methods using CASTEP. *Z. Kristallogr.* **2005**, *220*, 567.
(28) Pfrommer, B. G.; Cote, M.; Louie, S. G.; Cohen, M. L. Relaxation of Crystals with the Quasi-Newton Method. *J. Comput. Phys.* **1997**, *131*, 133.
(29) Schatschneider, B.; Liang, J. J. Simulated pressure response of crystalline indole. *J. Chem. Phys.* **2011**, *135*, 164508.
(30) Perdew, J. P.; Burke, K.; Ernzerhof, M. Generalized Gradient Approximation Made Simple. *Phys. Rev. Lett.* **1996**, *77*, 3865.
(31) Tkatchenko, A.; Scheffler, M. Accurate Molecular Van Der Waals Interactions from Ground-State Electron Density and Free-Atom Reference Data. *Phys. Rev. Lett.* **2009**, *102*, 073005.
(32) Tkatchenko, A.; Romaner, L.; Hofmann, O. T.; Zojer, E.; Ambrosch-Draxl, C.; Scheffler, M. van der Waals Interactions Between Organic Adsorbates and at Organic/Inorganic Interfaces. *MRS Bull.* **2010**, *35*, 435.
(33) Schatschneider, B.; Liang, J. J.; Jezowski, S.; Tkatchenko, A. Phase transition between cubic and monoclinic polymorphs of the tetracyanoethylene crystal: the role of temperature and kinetics. *CrystEngComm* **2012**, *14*, 4656.
(34) Burke, K. Perspective on density functional theory. *J. Chem. Phys.* **2012**, *136*, 150901.
(35) CrystalExplorer, version 2.2; Wolff, S. K., Grimwood, D. J., McKinnon, J. J., Turner, M. J., Jayatilaka, D., Spackman, M. A., Eds.; University of Western Australia: Australia, 2010.
(36) McKinnon, J. J.; Jayatilaka, D.; Spackman, M. A. Towards quantitative analysis of intermolecular interactions with Hirshfeld surfaces. *Chem. Commun.* **2007**, 3814.
(37) Spackman, M. A.; Jayatilaka, D. Hirshfeld surface analysis. *CrystEngComm* **2009**, *11*, 19.
(38) Podeszwa, R. B.; Rice, M.; Szalewicz, K. Predicting Structure of Molecular Crystals from First Principles. *Phys. Rev. Lett.* **2008**, *101*, 115503.
(39) von Lilienfeld, O. A.; Tkatchenko, A. Two- and three-body interatomic dispersion energy contributions to binding in molecules and solids. *J. Chem. Phys.* **2010**, *132*, 234109.
(40) Northrup, J. E.; Tiago, M. L.; Louie, S. G. Surface energetics and growth of pentacene. *Phys. Rev. B* **2002**, *66*, 121404.
(41) Schatschneider, B.; Phelps, J.; Jezowski, S. A new parameter for classification of polycyclic aromatic hydrocarbon crystalline motifs: a Hirshfeld surface investigation. *CrystEngComm.* **2011**, *13*, 7216.
(42) Drickamer, H. G.; Frank, C. W. *Electronic Transitions and the High Pressure Chemistry and Physics of Solids*; Chapman and Hall: London, 1973.
(43) Desiraju, G. R.; Gavezzotti, A. Crystal Structures of Polynuclear Aromatic Hydrocarbons. Classification, Rationalization and Prediction from Molecular Structure. *Acta Crystallogr.* **1989**, *B45*, 473.
(44) Fabbiani, P.; Allan, D. R.; Parsons, S.; Pulham, C. R. Exploration of the high-pressure behaviour of polycyclic aromatic hydrocarbons: naphthalene, phenanthrene and pyrene. *Acta Cryst. B* **2006**, *B62*, 826.
(45) Sondermann, U.; Kutoglu, A.; Bässler, H. X-ray diffraction study of the phase transition in crystalline tetracene. *J. Phys. Chem.* **1985**, *89*, 1735.
(46) Grimme, S. Do Special Noncovalent π-π Stacking Interaction Really Exist? *Angew. Chem., Int. Ed.* **2008**, *47*, 3430.
(47) Nicol, M.; Yin, G. Z. Organic Chemistry at High Pressure: Can Unsaturaterd bonds Survive 10 GPa. *J. Phys. (Coll)* **1984**, *45*, c8−163.
(48) Ishibash, S. First-principles electronic-band calculations on organic conductors. *Sci. Technol. Adv. Mater.* **2009**, *10*, 024311.
(49) Adamo, C.; Barone, V. Toward reliable density functional methods without adjustable parameters: The PBE0 model. *J. Chem. Phys.* **1999**, *110*, 6158.
(50) Paier, J.; Marsman, M.; Hummer, K.; Kresse, G.; Gerber, I. C.; Ángyán, J. G. Screened hybrid density functionals applied to solids. *J. Chem. Phys.* **2006**, *124*, 154709.
(51) Heyd, J.; Scuseria, G. E.; Ernzerhof, M. Hybrid functionals based on a screened Coulomb potential. *J. Chem. Phys.* **2003**, *118*, 8207.
(52) Samara, G. A.; Drickamer, H. G. Effect of Pressure on the Resistance of Fused-Ring Aromatic Compounds. *J. Chem. Phys.* **1962**, *37*, 474.